Power and Resource Allocation for Downlink Pilot Based Cell-Free Integrated Sensing and Communication Systems

Jiangwei Liao, Huiling Zhu, *Senior Member, IEEE*, Fangyuan Chen, Jiangzhou Wang,*Fellow, IEEE* and Changrun Chen

***Abstract*—In this paper, an integrated sensing and communication (ISAC) system was proposed under cell-free architecture with different power allocation schemes for both communication and sensing functions. In addition to using uplink (UL) pilot transmission for channel estimation, a group of pre-designed orthogonal downlink (DL) pilot sequences are inserted and transmitted from each cooperative access point (AP) towards the user equipments (UEs). The inserted DL pilots in cell-free ISAC are utilized for both channel estimation in communication and cooperative localization in radar sensing. Based on the ISAC strategy, a power allocation scheme is proposed with the objective of minimizing the maximum channel estimation error for each user, under the power constraints of APs and minimum mean square error constraints of the localization. The full-power scheme which APs consume all the available power during the DL phase is also studied and analyzed. The performance of the proposed ISAC strategy is evaluated under a realistic highway scenario, and compared to the existing non-DL strategies. Additionally, we investigate the impact of the pilot ratio under a constrained signal length, as well as the impact of the pilot proportion that the pilot length to the entire signal frame length. Simulation results show that the performances of both channel estimation and localization can be significantly improved at a relatively low cost of extra power needed for APs. Moreover, the analysis provides insights into optimizing the DL/UL pilot ratio and pilot proportion which can significantly enhance both channel estimation and localization accuracy, while ensuring sufficient resources remain available for data payload.**

***Index Terms*—Integrated sensing and communication, cell-free communication, collaborative localization, power allocation, pilot ratio.**

I. Introduction

FOR decades, communication and radar sensing have operated on separate networks. However, with a growing number of physical sensing devices connecting to the Internet, the upcoming sixth-generation (6G) network faces a significant demand for integrating communication and sensing within a unified network [1], [2]. The coordination needs to offer high data rate transmission for communication devices while providing precise localization or tracking for user equipment (UE) in radar systems. With advancements in waveforms, antennas and signal processing technologies, integrated sensing and Communication (ISAC), also known as joint communication and sensing (JCAS), has emerged as a promising approach in multi-antenna based wireless networks.

With multiple antennas implemented at base stations (BSs), the monostatic ISAC system can operate without requiring cooperation between BSs [3]–[6]. However, this approach may lead to significant interference between BSs.

In contrast, the multi-static ISAC system, which cooperate multiple BSs in different positions and transmission paths, can offer a larger possibility of coverage and better performance than co-located radar system because of diversity gain and perspectives provided by access point (AP) observations with the same power consumption, compared to the mono-static radar system [7]. The multi-static radar system depends on not only bandwidth and receiver signal-to-noise ratio (SNR) as the conventional mono-static radar system, but also the number of bi-static channels and the geometric dilution of precision (GDOP) which reflects the geometry among the radar nodes to the targe [8], [9]. In [9] and [10], both works have achieved 1m^2 lower localization estimation error in narrow bandwidth signals within different bi-static channel number and GDOP parameters.

When cooperating with multi-static BSs, transmitting unsynchronized signals from different nodes will lead to interference and transmission error. To deal with the synchronization requirement of the signals transmission among multiple transmitters and receivers, cell-free distributed multiple input multiple output (MIMO) has been considered as a promising solution [11]–[14]. In cell-free distributed MIMO networks, separated multiple distributed APs are connected to a central processing unit (CPU). The APs can cooperate and share information with each other, serving each UE at the same time-frequency resource.

In the UL phase and radar receivers, the APs are synchronized within a shared clock information from the CPU [14]. In our system, one of the fundamental methods which known as the two-way message exchange synchronization, is utilized. In this synchronization algorithm, a radar node A which requires to be synchronized, sending a synchronization message to a reference node. The reference node records the reception time of the message and replies, providing timestamps for both reception and transmission. By analyzing the timestamps from the reply message, node A can derive the relative clock skew and offset of itself with respect to the reference node [15].

J. Liao, H. Zhu, and C. Chen are with the School of Engineering, University of Kent, Canterbury CT2 7NT, U.K. (e-mail: jl804,h.zhu,c.chen@kent.ac.uk), F. Chen is with Jinyichang Science&Technology Co., Lt, China (e-mail: cfy@jinchanggps.com), J. Wang is with Southeast University, Nanjing, China (e-mail: j.z.wang@kent.ac.uk) This work was supported in part by the European Commissionas Horizon Europe Marie SkAodowska-Curie Postdoctoral Fellowship-UKRI guarantee under Grant EP/Y027558/1 (Corresponding author: Changrun Chen).

As in the cell-free networks where all the distributed APs are connected and share their clock information, we assume that the time and phase of the echoes are able to be synchronized and aligned at each AP receivers by considering the CPU as the reference node.

In the DL phase, each AP estimates the timing errors based on the UL training and transmit the DL signal with advancing or delaying [16], additional cyclic prefix (CP) which is longer than relative timing errors among APs can also alleviate the DL asynchronous interference at the UE. Therefore, the synchronization issue in both UL and DL can be resolved among APs via the assistance of the CPU.

Moreover, as APs in cell-free network are widely spread and are able to cover a large area, each AP can be considered as a non-co-located radar transmitter and receiver to form a multi-static ISAC system. To implement cell-free ISAC, two approaches have been proposed in the existing research. One approach was to directly utilize the data payload as radar waveform. However, the communication data sequences were not optimized for sensing purpose. For example, the transmitted information data payloads were random and lack high orthogonality, which led to significant detection errors and high false alarm rates. Deterministic radar sensing sequences with good orthogonality were required for distributed radar system, allowing for proper extraction and identification during signal processing [17]. The other approach involved inserting additional segments into the transmission sequence specially for sensing tasks [18], [19]. These extra sequences were specially designed to be orthogonal to each other. However, this method did not improve communication performance, as the communication and sensing function are independent and do not improve each other. Thus, the space efficiency of the signal is reduced.

This motivates our work, where the pre-designed pilots are inserted into the downlink (DL) transmission of the cell-free ISAC system. Even though the existing cell-free networks typically do not use DL pilots due to channel hardening [20], [21], the recent research [22]–[24] pointed out that the channel hardening assumption may not be reliable when analyzing the cell-free massive MIMO networks since the UEs are primarily served by its closest APs, despite the large total number of APs deployed in the coverage area. To obtain more accurate channel estimation information (CSI), during DL transmission in the cell-free ISAC, APs send pre-designed DL pilots at the same time-frequency resources to the corresponding UE, leveraging the CSI estimated from the uplink (UL) training. These DL training sequences, generated with high orthogonality, are not only used for channel estimation enhancement in communication but also for localization in radar sensing.

However, a trade-off problem emerges. The resource allocation schemes need to balance the performance between the communication and radar sensing in order to achieve the requirements. The trade-off for cell-free ISAC system in this paper becomes the power allocation problem between pilot and data payload in DL. This trade-off can be balanced by implementing the transmitted pilot sequences for channel estimation and localization requirement while guaranteeing adequate power used for the following data transmission.

A. Contributions

Unlike the existing works that considered additional sensing beams or radar sequences for target detection and localization, this paper considers multi-static localization for ISAC in DL cell-free massive MIMO networks by inserting additional DL training sequences from APs to UEs. We consider UE and target as a unified object, where the UE being served is simultaneously detected and located, like [25]. There are four phases during the system processing: *(i)* UL training and channel estimation at APs, *(ii)* UL data transmission from UEs to APs, *(iii)* DL training at UEs and sensing at APs, *(iv)* DL data transmission from APs to UEs. Our work focuses on the third phase, aiming to improve the channel estimation performance and implement collaborative localization via the inserted DL training sequences. Different from the traditional cell-free ISAC massive MIMO system, at which APs are utilized as either ISAC transmitter or radar echo receiver, we assume all the APs are ISAC transceivers to transmit ISAC signals to UEs as well as receive radar echoes reflected by UEs during DL.

The communication metric is measured by the normalized channel estimation error which is estimated with the DL sequences at UE with the knowledge of the pre-obtained UL CSI, and the impact of the channel estimation error on the DL data transmission rate is also evaluated. The radar sensing metric is represented by the theoretical lower bound, Cramér–Rao lower bound (CRB), of the collaborative localization results from the received echoes at each AP. Two power allocation schemes are developed with the objective of minimizing the maximum DL channel estimation error for each UE while satisfying the requirement of the maximum sensing error, under the power constraints of each AP. The impacts among the different ratios on DL to UL pilot lengths, and different pilot proportions on the pilot length to the entire signal frame length, are also investigated with respect to the power allocation scheme. The main contributions of this papers are summarized as follows:

- A cell-free ISAC massive MIMO system with inserted DL training sequences is proposed, where during the DL training phase, every AP sends DL pilots, based on the CSI matrices obtained from advance UL training, to UEs for improving channel estimation. In the meantime, when the DL sequences are reflected by the UEs, all the APs receive the echoes and transmit to CPU via fronthaul to perform target localization.
- To minimize the channel estimation error for each system-UE channels while satisfying the requirement of radar sensing constraints, one convex optimization-based power allocation algorithm is proposed. To evaluate the performance of the proposed system strategy under the optimized power allocation scheme, a full-power scheme, at which each AP utilizes all of its allocated power for DL transmission, is also raised and compared. Four performance aspects are compared between the proposed and the existing cell-free ISAC systems: the variance of normalized channel estimation error, the DL data transmission rate corresponding to the channel estimated errors, the average localization lower bound under the

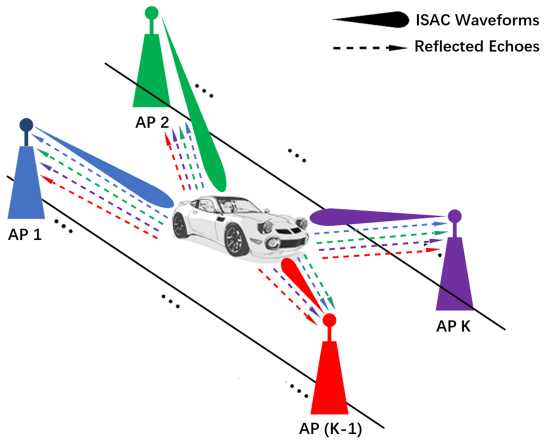

Fig. 1: Illustration of the cell-free ISAC system with multi-static sensing.

same radar signal SNR, and the power consumption of the system.

- We investigate the impact of the inserted pilot sequences with different DL/UL ratio and pilot proportion. The system performance for the average of a thousand randomly deployed UEs with different ratios and proportions are studied and compared, in order to minimize the pilot overhead when achieving the requirement on both communication and radar metrics.

The rest of this paper is organized as follows. In Section II, we demonstrate the ISAC system model in cell-free massive MIMO architecture, define the basic parameters and signal models of communication and radar. Section III describes the estimation algorithms for DL channel estimation and multi-static localization, and the proposed power allocation problem is devoted. Section IV presents the numerical results under different system strategies and power allocation schemes, the performance of different pilot ratio are also compared and discussed. Finally, Section V concludes the paper.

B. Notations

The following mathematical notions are used in this paper. x, $\mathbf{x}$, $\mathbf{X}$ and $\mathcal{X}$ are denoted by scalar, vector, matrix and set, respectively. $|\cdot|$ denotes the Euclidean norm for a complex vector. $(\cdot)^T$, $(\cdot)^*$ and $(\cdot)^H$ respectively denote the transpose, conjugate and conjugate transpose. $\mathbb{C}^M$ and $\mathbb{C}^{M\times N}$ represent the set of $M\times 1$ and $M\times N$ complex vectors, respectively. $\{\mathbf{x}_{ij}\}$ denotes all admissible $\{i,j\}$ for $\mathbf{x}_{ij}$. $\mathrm{tr}(\cdot)$ denotes the trace of a matrix. $\mathrm{Cov}(x_1,x_2)$ is denoted by the covariance of two random complex variables x_1 and x_2. $\mathbb{E}\{\cdot\}$ and $\mathbb{V}\{\cdot\}$ denotes the expectation and variance of a random complex variable. $\mathbf{x}\sim\mathcal{CN}(\mu,\sigma^2)$ represent that $\mathbf{x}$ is a complex symmetric Gaussian random variable with mean μ and variance σ^2.

II. System and Signal Model

A. System Model

We consider an ISAC system with DL training, DL communication and multi-static sensing in cell-free network, as shown in Fig.1. In this system, a total number of M APs and K UEs are deployed in a certain coverage area. Let $\mathcal{M}=\{1,2,\cdots,M\}$ and $\mathcal{K}=\{1,2,\cdots,K\}$ represent the sets of APs and UEs, respectively. Each AP is equipped with multiple circulators and hybrid couplers, facilitating vertical polarization for transmitting and horizontal polarization for receiving. The antenna structure creates significant isolation between transmitted and received signals, which enables the implementation of full-duplex hardware capable of achieving RF isolation more than 90 dB at 2.4 GHz [26], [27]. The APs serve as both ISAC transmitter and radar receiver, while UEs are treated as DL communication terminals and point-like targets. Both APs and UEs are equipped with a single-antenna transmitter and a single-antenna receiver. Thus, single-carrier (SC) waveforms are considered as the ISAC signal in the system model because of one antenna only. Moreover, compared to the conventional OFDM waveforms, the SC can avoid the high peak-to-average power ratio (PAPR) which leads to serious nonlinear distortion in radar signals [28], [29], therefore, the PAPR reduction techniques are not required at APs, which simplifies the design of single-antenna APs and contributes to reduced hardware cost. All APs are connected to a CPU via fronthaul, which allows APs to synchronously share their transmitted and received signals among others and implements signal processing with high performance unit.

The coverage area is considered as a coordinate system on a 2-D plane. The APs are uniformly deployed on both sides of the road, which the position of the m-th AP is given by $(m_x,\ m_y)$. The UEs are randomly distributed in the certain range, which the position denoted as $(k_x,\ k_y)$ for the k-th UE.

In addition to the DL channel estimation for improving the CSI values at UE, the DL training sequences hit the target UE and are reflected by its surface, received by all surrounding APs. The radar signal processing is performed in the CPU for locating the position of the target UE. Since these orthogonal sequences are designed in advance, and all APs share and know the sequences of others, we assume that the CPU can recognize the received echoes from the AP reflected by the corresponding UE. The coherence interval length for ISAC signal is $\tau_{\text{ISAC}}=\tau_p+\tau_c=\tau_{u,p}+\tau_{u,c}+\tau_{d,p}+\tau_{d,c}$, which the total length of the pilot sequence τ_p can impact the performance of the system.

The distance between the m-th AP and the k-th UE is denoted by $D_{m,k}=\sqrt{(k_x-m_x)^2+(k_y-m_y)^2}$. The propagation time defines as the time interval for ISAC signals transmitted from the m-th AP, reflected by the k-th UE, and then received by the n-th AP, which is represented by $\tau_{m,k,n}=\frac{D_{m,k}+D_{n,k}}{c}$, where c is the speed of light. Moreover, the system introduces the UE's radar crossing section (RCS) $\zeta_{m,n}$ for each AP to describe the power scattered back to the radar, and we assume that it is deterministic.

B. Cell-Free Communication with Channel Estimation

We consider the impacts of both small-scale and large-scale fading. Denote $g_{m,k}=\sqrt{\beta_{m,k}}h_{m,k}$ as the instantaneous CSI between the m-th AP and the k-th UE, where $\beta_{m,k}$ is the large-scale fading and $h_{m,k}$ represents the small-scale

fading. Suppose the large-scale fading coefficients $\{\beta_{m,k}\}$ are constant during every coherence intervals, therefore the values can be estimated in prior and known. Assume that the small-scale fading coefficients $\{h_{m,k}\}$ are identically independent distributed (i.i.d.) random variables (RVs) $h_{m,k} \sim \mathcal{CN}(0,1)$.

To transmit the DL pilot sequences to UE, the system requires the primary CSI between the m-th AP and k-th UE from UL training of phase *(i)*. During the UL training, every UE sends its own training sequences $\boldsymbol{\phi}$ to all the APs in the coverage area. The surrounding APs need to estimate the channel when they received the UL pilots.

Define $\sqrt{\tau_{u,p}}\boldsymbol{\phi}_k \in \mathbb{C}^{\tau_{u,p}\times 1}$, where $||\boldsymbol{\phi}_k||^2 = 1$, as the UL training pilots sent by the k-th UE, we assume that any two UL training sequences are either identical or mutually orthogonal,

$$\boldsymbol{\phi}_k^H \boldsymbol{\phi}_{k'} = \begin{cases} 1 & \text{if } \boldsymbol{\phi}_k = \boldsymbol{\phi}_{k'}, \\ 0 & \text{otherwise} \end{cases} \tag{1}$$

Therefore, the m-th AP receives the UL training signal as follows

$$\mathbf{y}_{u_{m,k}} = \sqrt{\tau_{u,p}\rho_{u,p}} \sum_{k=1}^{K} g_{m,k}\boldsymbol{\phi}_k + \boldsymbol{w}_{u_m} \tag{2}$$

where $\rho_{u,p}$ represents the power of UL pilot symbol, $\boldsymbol{w}_{u_m}$ is the additive noise at the m-th AP during UL, within its elements are i.i.d. $\sim \mathcal{CN}(0,1)$ RVs.

To estimate the channel $g_{m,k}$, the received training signal $\mathbf{y}_{u_{m,k}}$ is projected onto known pilot sequence $\boldsymbol{\phi}_k^H$ locally at the m-th AP, which is given by

$$\begin{aligned} \check{\mathbf{y}}_{u_{m,k}} &= \boldsymbol{\phi}_k^H \mathbf{y}_{u_{m,k}} \\ &= \sqrt{\tau_{u,p}\rho_{u,p}} g_{m,k} + \sqrt{\tau_{u,p}\rho_{u,p}} \sum_{k' \neq k}^{K} g_{m,k'} \boldsymbol{\phi}_k^H \boldsymbol{\phi}_{k'} \\ &\quad + \boldsymbol{\phi}_k^H \boldsymbol{w}_{u_m} \end{aligned} \tag{3}$$

Although $\check{\mathbf{y}}_{u_{m,k}}$ does not suffice the channel estimation of $g_{m,k}$ because of the second term which is the UL pilot contamination effect, the assumption of (1) ensures that $\check{\mathbf{y}}_{u_{m,k}}$ is a sufficient statistic [12].

Based on the projection of the received UL training pilots in each AP, the minimum mean square error (MMSE) estimation [30] to the UL estimated CSI $\hat{g}_{m,k}$ between the m-th AP and the k-th UE is given as

$$\hat{g}_{m,k} = \frac{\sqrt{\tau_{u,p}\rho_{u,p}}\beta_{m,k}}{\tau_{u,p}\rho_{u,p}\sum_{k'=1}^{K}\beta_{m,k'}|\boldsymbol{\phi}_k^H\boldsymbol{\phi}_{k'}|^2 + 1} \check{\mathbf{y}}_{u_{m,k}} \tag{4}$$

Proof. See Appendix A.

The mean-square of the estimated channel gain is defined by $\gamma_{m,k}$ and given as

$$\begin{aligned} \gamma_{m,k} &\triangleq \mathbb{E}\{|\hat{g}_{m,k}|^2\} \\ &= \frac{\tau_{u,p}\rho_{u,p}\beta_{m,k}^2}{\tau_{u,p}\rho_{u,p}\sum_{k'=1}^{K}\beta_{m,k'}|\boldsymbol{\phi}_k^H\boldsymbol{\phi}_{k'}|^2 + 1} \end{aligned} \tag{5}$$

The channel estimation error is denoted as $\tilde{g}_{m,k} \triangleq g_{m,k} - \hat{g}_{m,k}$, therefore, the variance of UL channel estimation error is

$$\mathbb{V}\{\tilde{g}_{m,k}\} = \beta_{m,k} - \gamma_{m,k} \tag{6}$$

Proof. See Appendix B.

Similarly as the UL training, during the DL training phase, the pilots which are used by conjugate beamforming, sent from the m-th AP and intended to the k-th UE, is represented by $\boldsymbol{\psi}_k$, where $\|\boldsymbol{\psi}_k\|^2 = 1$. Assume that $\sqrt{\tau_{u,p}}\boldsymbol{\psi}_k \in \mathbb{C}^{\tau_{d,p}\times 1}$. These DL training sequences are also pre-designed to ensure that any two of them are either identical or mutually orthogonal,

$$\boldsymbol{\psi}_k^H \boldsymbol{\psi}_{k'} = \begin{cases} 1 & \text{if } \boldsymbol{\psi}_k = \boldsymbol{\psi}_{k'}, \\ 0 & \text{otherwise} \end{cases} \tag{7}$$

In order to coordinate all the APs form distributed MIMO system, precoding techniques which aim to enhance the signal strength and improve the relaibility of transmission, such as maximum ratio transmission (MRT), are often used at the receiver. Therefore, the transmitted signals between APs and UEs will be weighted by the CSI of the channel. Based on the pre-obtained CSI from the UL training, the $\tau_{d,p}\times 1$ DL training vector from the m-th AP to the serving UEs is formulated as

$$\mathbf{x}_m = \sqrt{\tau_{d,p}\rho_d} \sum_{k=1}^{K} \sqrt{\eta_{m,k}}\hat{g}_{m,k}^* \boldsymbol{\psi}_k \tag{8}$$

where ρ_d is the total power for every AP during DL training phase per symbol. To mitigate the influence of pilot contamination, $\eta_{m,k}$ is introduced as a control coefficient to adjust the allocated power of pilot transmission of the m-th AP. Each AP can only use their own power and cannot consume power from other APs or the CPU, therefore, the average power of transmitted DL training sequence at the m-th AP constraints:

$$\begin{aligned} &\mathbb{E}\left\{|\mathbf{x}_m|^2\right\} = \tau_{d,p}\rho_d \sum_{k=1}^{K} \eta_{m,k}\gamma_{m,k} \leq \tau_{d,p}\rho_d \\ &\text{therefore, } \sum_{k=1}^{K} \eta_{m,k}\gamma_{m,k} \leq 1 \end{aligned} \tag{9}$$

Correspondingly, the received pilot sequences at the k-th UE can be expressed as

$$\begin{aligned} \mathbf{y}_{d_k} &= \sum_{m=1}^{M} g_{m,k}\mathbf{x}_{m,k} + \sum_{k\neq k'}^{K}\sum_{m=1}^{M} g_{m,k}\mathbf{x}_{m,k'} + \boldsymbol{w}_{d_k} \\ &= \underbrace{\sqrt{\tau_{d,p}\rho_d}\boldsymbol{a}_k\boldsymbol{\psi}_k}_{\text{Desired Signal}} + \underbrace{\sqrt{\tau_{d,p}\rho_d}\sum_{k\neq k'}^{K}\boldsymbol{a}_{k'}\boldsymbol{\psi}_{k'}}_{\text{Inter-user Interference}} + \boldsymbol{w}_{d_k} \end{aligned} \tag{10}$$

where

$$\boldsymbol{a}_{k'} = \sum_{m=1}^{M} \sqrt{\eta_{m,k'}} g_{m,k}\hat{g}_{m,k'}^*, \qquad k' = 1,\ldots,K \tag{11}$$

describes the effective channel gain which combines all the DL channels from APs to the k-th UE [24]. The additive noise $\boldsymbol{w}_{d_k} \sim \mathcal{CN}(0,1)$ at the AP receiver is Gaussian distributed.

Similar to (4), the received DL training sequences at the k-th UE receiver will be processed by projecting them onto the known DL pilots $\boldsymbol{\psi}_k^H$,

$$\begin{aligned}\check{\mathbf{y}}_{d_k} &= \boldsymbol{\psi}_k^H \mathbf{y}_{d_k} \\ &= \sqrt{\tau_{d,p}\rho_{d,p}}\boldsymbol{a}_k + \sqrt{\tau_{d,p}\rho_{d,p}}\sum_{k'\neq k}^{K}\boldsymbol{a}_k'\boldsymbol{\psi}_k^H\boldsymbol{\psi}_{k'} \\ &+ \boldsymbol{\psi}_k^H\boldsymbol{w}_{d_k}\end{aligned} \tag{12}$$

The second term comes from the DL pilot contamination. Although the pilot sequences are pre-designed and ensure orthogonality as shown in (7), when the number of UEs are more than the number of training sequences, the pilots will be reused and lead to the interference.

Therefore, based on the projection in UE, the linear MMSE estimation of a_k is derived as,

$$\hat{\boldsymbol{a}}_k = \frac{\mathrm{Cov}\{\boldsymbol{a}_k, \check{\mathbf{y}}_{d_k}\}}{\mathbb{V}\{\check{\mathbf{y}}_{d_k}\}}(\check{\mathbf{y}}_{d_k} - \mathbb{E}\{\check{\mathbf{y}}_{d_k}\}) + \mathbb{E}\{\boldsymbol{a}_k\} \tag{13}$$

where [24]

$$\mathrm{Cov}\{\boldsymbol{a}_k, \check{\mathbf{y}}_{d_k}\} = \sqrt{\tau_{d,p}\rho_{d,p}}\sum_{m=1}^{M}\eta_{m,k}\gamma_{m,k}\beta_{m,k} \tag{14}$$

$$\mathbb{V}\{\check{\mathbf{y}}_{d_k}\} = 1 + \tau_{d,p}\rho_{d,p}\sum_{m=1}^{M}\sum_{k'=1}^{K}\eta_{m,k'}\gamma_{m,k'}\beta_{m,k}|\boldsymbol{\psi}_k^H\boldsymbol{\psi}_k'|^2 \tag{15}$$

$$\mathbb{E}\{\check{\mathbf{y}}_{d_k}\} = \sqrt{\tau_{d,p}\rho_{d,p}}\sum_{m=1}^{M}\sqrt{\eta_{m,k}}\gamma_{m,k} \tag{16}$$

$$\mathbb{E}\{\boldsymbol{a}_k\} = \sum_{m=1}^{M}\sqrt{\eta_{m,k}}\gamma_{m,k} \tag{17}$$

By applying the effective DL channel gain $\boldsymbol{a}_k$ and the linear MMSE estimation $\hat{\boldsymbol{a}}_k$, the variance of the zero-mean DL channel estimation error is defined as $\mathbb{V}\{\tilde{\boldsymbol{a}}_k\} = \mathbb{V}\{\boldsymbol{a}_k\} - \mathbb{V}\{\hat{\boldsymbol{a}}_k\}$, within a similar proof of (6) as shown in Appendix B. The variance of the effective DL channel is expressed by $\mathbb{V}\{\boldsymbol{a}_k\} = \sum_{m=1}^{M}\eta_{m,k}\beta_{m,k}\gamma_{m,k}$, while $\mathbb{V}\{\hat{\boldsymbol{a}}_k\} = \frac{\tau_{d,p}\rho_d(\sum_{m=1}^{M}\eta_{m,k}\beta_{m,k}\gamma_{m,k})^2}{1+\tau_{d,p}\rho_d\sum_{k'=1}^{K}\sum_{m=1}^{M}\eta_{m,k'}\beta_{m,k}\gamma_{m,k'}|\boldsymbol{\psi}_k^H\boldsymbol{\psi}_{k'}|^2}$ is the variance of the estimated DL channel [24]. Therefore, we have

$$\mathbb{V}\{\tilde{\boldsymbol{a}}_k\} = \frac{\sum_{m=1}^{M}\eta_{m,k}\beta_{m,k}\gamma_{m,k}}{1+\tau_{d,p}\rho_d\sum_{k'=1}^{K}\sum_{m=1}^{M}\eta_{m,k'}\beta_{m,k}\gamma_{m,k'}|\boldsymbol{\psi}_k^H\boldsymbol{\psi}_{k'}|^2} \tag{18}$$

The variance of the DL channel estimation error is considered as the communication metric for measuring the performance of the cell-free ISAC system with the introduced DL training sequences.

C. Collaborative Radar Sensing

In our proposed system, the DL training sequences are used for not only communication channel estimation but also radar sensing waveform. We assume that every AP is full-duplex so they can transmit radar waveform while receive reflected echoes. In a cell-free ISAC system, multiple APs work as multiple radar agents. Within the joint processing algorithms, e.g. matched filters [10], the geometric diversity greatly improves the ability to distinguish targets due to different signal paths, time delays and angles observed by multiple APs. [10] proved that a higher probability of target detection can be achieved by multi-static radar systems with multiple radar agents at the same radar SNR, compared to the bi-static radar with only two radar agents. Consequently, we assume that the interference caused by signal overlap and time misalignment can be effectively mitigated.

The received echoes $\boldsymbol{r}_{m,k,n}$, which transmitted from the m-th AP transmitter, reflected by the k-th UE target and received at the n-th AP receiver, consist of the desired part and the undesired part. The undesired part is composed of three signals, the inter-waveform interference caused by the training pilot contamination, the clutter due to the scatterings from permanent and temporary objects, and the noise. For simplification, we consider that the undesired part except the noise can be obtained in advance and removed from the echoes by radar signal processing at the AP receiver. The separation of the echoes is based on distinct round-trip delay. Since the pilot sequences are designed in advance in order to ensure good orthogonality, every APs are linked to CPU and can share their information with each other, we assume that each AP receivers can recognize the echoes reflected by the which target and transmitted from which AP. The permanent objects such as buildings and trees are assumed to be fixed, which their positions and reflectivities can be modeled and known in advance. The temporary objects, like the moving vehicles and passers-by, are also served by the cell-free ISAC system, therefore their positions are detected and obtained by all the APs. The continuous-time signal of the DL pilot sequence in an AP-UE-AP link, which is transmitted from the m-th AP, reflected by the k-th UE and received by the n-th AP is expressed as

$$\boldsymbol{r}_{m,k,n}(\tau) = \sqrt{\alpha_{m,n}p_{m,k}}\zeta_{m,n}\boldsymbol{x}_{m,k}(\tau - \tau_{m,k,n}) + \boldsymbol{w}_{r_{m,k,n}} \tag{19}$$

where $\alpha_{m,n} = \frac{\lambda_c^2}{(4\pi)^3 D_{m,k}^2 D_{n,k}^2}$ is the variation in signal strength due to the distance-dependent two-way path loss, λ_c is the wavelength of the signal [31], $p_{m,k} = \mathbb{E}\left\{|\mathbf{x}_{m,k}|^2\right\}$ represents the power of pilot sequences sent from the m-th AP to the k-th UE. As a result, the echoes received at the n-th AP is denoted as

$$\begin{aligned}\boldsymbol{r}_n(\tau) = &\sum_{m=1}^{M}\sqrt{\alpha_{m,n}p_{m,k}}\zeta_{m,n}\boldsymbol{x}_{m,k}(\tau - \tau_{m,k,n}) \\ &+ \sum_{k'\neq k}^{K}\sum_{m=1}^{M}\sqrt{\alpha_{m,n}p_{m,k'}}\zeta_{m,n}\boldsymbol{x}_{m,k'}(\tau - \tau_{m,k',n}) \\ &+ \boldsymbol{w}_r\end{aligned} \tag{20}$$

Since the DL pilots are used for dual-functions, the power to radar sensing is the same as the power to communication channel estimation. The noise at the AP receiver of the reflected sequence is $\boldsymbol{w}_{r_{m,k,n}} \sim \mathcal{CN}(0, \sigma_w^2)$.

The channel (m, k, n) is the propagation path from the m-th AP transmitter to the k-th target and from the k-th target to

the n-th AP receiver. The SNR of the radar channel (m,k,n) is

$$\text{SNR}_{r_{m,k,n}} = \frac{\alpha_{m,n} p_{m,k} |\zeta_{m,n}|^2}{\sigma_w^2} \tag{21}$$

Although the target is moving, we suppose that the target's velocity is lower than the sensing period during the DL processing time interval. Thus, the detected target position and speed are considered static, the cell-free ISAC system can track and predict the target during the ISAC signal transmission without additional feedback from the target.

Within the known pilots and radar signals, the channel parameters such as angle-of-arrival (AOA), angle-of-departure (AOD) and propagation delay can be extracted. The angle can be obtained when a group of antenna array is implemented at the receiver side, while the propagation distance can be computed based on the received signal signal strength [32]. The time-difference-of-arrival (TDOA) is used for localization by measuring the time arrival difference at multiple receivers. Based on the different arrival times, TDOA forms geometrical expressions of hyperboloids in 3D or hyperbolas in 2D [33], [34]. The intersection of the hyperboloids or hyperbolas pins the position of the target. The proposed system produces the actual UE positions by the TDOA because TDOA achieves better performance compared to other methods such as time of arrival (TOA) [35] and angle of arrival (AOA) [36].

In order to measure the radar function directly, we evaluate the localization performance in terms of the MSE of target's position estimation. We introduce CRB [30] to find the lowest bound MSE for unknown parameters that any unbiased estimator can achieve, that is $\text{MMSE}(\boldsymbol{r}_{m,k,n}) \geq \text{CRB}(\boldsymbol{r}_{m,k,n})$. Computing the CRB values of the radar estimator means to find the best signal processing results under the whole obtained signal information with the lowest MSE estimator.

Even though there are several studies [37], [38] consider the CRB calculation with the non-line-of-sight paths between the transmitter to the target or the target to the receiver via the biased observations, our model only concerns the best collaborative sensing results it can achieve. Therefore, for the localization with the lowest error, we suppose that all the signals are line-of-sight in the radar waveform transmission model, which means every signals are directly sent and received without reflecting by more than one object.

Assume the position of the k-th UE is estimated on a 2-D plane for the ISAC system, the unknown vector estimated by radar is defined as $\boldsymbol{\theta}_k = [k_x, k_y, \boldsymbol{\zeta}]^T$, where k_x and k_y respectively are UE k's coordinate system values on the 2-D plane, $\boldsymbol{\zeta} = [\zeta_{1,1}, \cdots, \zeta_{1,n}, \zeta_{2,1}, \cdots, \zeta_{m,n}]^T$. Given $\hat{\boldsymbol{\theta}}_k$ as the estimated result of the k-th AP receiver for the unbiased estimator, the estimate satisfies the inequality

$$\mathbb{E}\{(\hat{\boldsymbol{\theta}}_k - \boldsymbol{\theta}_k)(\hat{\boldsymbol{\theta}}_k - \boldsymbol{\theta}_k)^T\} \geq \boldsymbol{J}^{-1}(\boldsymbol{\theta}_k) \tag{22}$$

where the $\boldsymbol{J}^{-1}(\boldsymbol{\theta}_k)$ is the Fisher Information matrix (FIM) given by

$$\boldsymbol{J}(\boldsymbol{\theta}_k) = \mathbb{E}\left\{ \frac{\partial \log f(\boldsymbol{r}_k|\boldsymbol{\theta}_k)}{\partial \boldsymbol{\theta}_k} \left(\frac{\partial \log f(\boldsymbol{r}_k|\boldsymbol{\theta}_k)}{\partial \boldsymbol{\theta}_k} \right)^T \right\} \tag{23}$$

where $f(\boldsymbol{r}_k|\boldsymbol{\theta}_k)$ is the conditional joint probability density function (pdf) of the radar observation of the k-th UE $\boldsymbol{r}_k = \{r_{1,k,1}, r_{1,k,2}, \cdots, r_{M,k,N}\}$. Therefore, based on the received radar signal in (19), the logarithmic function of the conditional pdf is expressed as

$$\begin{aligned} \log f(\boldsymbol{r}_k|\boldsymbol{\theta}_k) \propto & -\frac{1}{\sigma_w^2} \sum_{m=1}^{M} \sum_{n=1}^{N} |\boldsymbol{r}_{m,k,n}(\tau) \\ & - \sqrt{\alpha_{m,n} p_{m,k}} \zeta_{m,n} \boldsymbol{x}_{m,k}(\tau - \tau_{m,k,n})|^2 d\tau \end{aligned} \tag{24}$$

Since we only care the localization MSE on the coordinate system of the target, the 2×2 upper left block sub-matrix $\mathbf{C}_{k_x,k_y}$ of the inversed FIM $\boldsymbol{J}^{-1}(\boldsymbol{\theta}_k)$ is derived as a function of the power allocation $\boldsymbol{p}_{tx,k}$ by the M-transmitter-N-receiver multi-static radar system [39], [40],

$$\mathbf{C}_{k_x,k_y}(\boldsymbol{p}_{tx,k}) = \left\{ \sum_{m=1}^{M} p_{m,k} \begin{bmatrix} r_{a_m} & r_{c_m} \\ r_{c_m} & r_{b_m} \end{bmatrix} \right\}^{-1} \tag{25}$$

where

$$\begin{aligned} r_{a_m} =& \xi_m \sum_{n=1}^{N} \alpha_{m,n} |\zeta_{m,n}|^2 \left(\frac{m_x - k_x}{D_{m,k}} + \frac{n_x - k_x}{D_{n,k}} \right)^2, \\ r_{b_m} =& \xi_m \sum_{n=1}^{N} \alpha_{m,n} |\zeta_{m,n}|^2 \left(\frac{m_y - k_y}{D_{m,k}} + \frac{n_y - k_y}{D_{n,k}} \right)^2, \\ r_{c_m} =& \xi_m \sum_{n=1}^{N} \alpha_{m,n} |\zeta_{m,n}|^2 \left(\frac{m_x - k_x}{D_{m,k}} + \frac{n_x - k_x}{D_{n,k}} \right) \\ & \times \left(\frac{m_y - k_y}{D_{m,k}} + \frac{n_y - k_y}{D_{n,k}} \right), \\ \xi_m =& \frac{8\pi^2 B_m^2}{\sigma_w^2 c^2}, \end{aligned} \tag{26}$$

where B_m is the effective bandwidth of the transmitted pilot sequence from the m-th AP, $\boldsymbol{p}_{tx,k} = [p_{1,k}, p_{2,k}, \cdots, p_{M,k}]^T$ is the power vector for every APs to the k-th UE. The trace of $\mathbf{C}_{k_x,k_y}(\boldsymbol{p}_{tx,k})$ gives a lower bound on the sum of the target's x and y localization MSEs [39], which the MSE of the multi-static radar on coordinate system can be expressed as

$$\begin{aligned} \sigma^2_{k_x,k_y}(\boldsymbol{p}_{tx,k}) =& tr\left\{ \mathbf{C}_{k_{k_x,k_y}}(\boldsymbol{p}_{tx,k}) \right\} \\ =& \frac{(\boldsymbol{r}_a + \boldsymbol{r}_b)^T \boldsymbol{p}_{tx,k}}{\boldsymbol{p}_{tx,k}^T (\boldsymbol{r}_a \boldsymbol{r}_b^T - \boldsymbol{r}_c \boldsymbol{r}_c^T) \boldsymbol{p}_{tx,k}} \end{aligned} \tag{27}$$

where $\boldsymbol{r}_a = [r_{a_1}, r_{a_2}, \cdots, r_{a_m}]^T$, $\boldsymbol{r}_b = [r_{b_1}, r_{b_2}, \cdots, r_{b_m}]^T$ and $\boldsymbol{r}_c = [r_{c_1}, r_{c_2}, \cdots, r_{c_m}]^T$.

The equation for the CRB of the collaborative sensing offers the sensing metric to measure the performance of the cell-free ISAC system after introducing the DL training sequences in radar sensing. The radar requirements of the localization error measured in meter is used as the optimization constrain in the next section. According to (21), (25) and (26), the CRB is also related to and can be changed by the SNR values at the radar receivers.

III. Power Control Algorithms

In Section II-B and II-C, we have derived the variance of channel estimation error as the communication metric and the CRB of the localization estimator as the radar metric. In this section, we introduce the power allocation strategies

for the proposed ISAC system where a group of DL training sequences are utilized in the DL training phase for communication channel estimation at UEs and the radar localization at AP receivers. Two power allocation strategies are discussed: the optimized power allocation based on successive convex approximation (SCA), and the full-power (also named water-filling) allocation. The former aims to minimize the objective under constraints with as little power as possible, while the latter consumes all the power each AP has without considering signal interference and energy conservation.

In this section, we minimize the normalized channel estimation error in DL training phase, denoted by $\frac{\mathbb{V}\{\tilde{\boldsymbol{a}}_k\}}{\mathbb{E}|\boldsymbol{a}_k|^2}$, where the variance of error is normalized by its DL channel channel gain $\mathbb{E}\{|\boldsymbol{a}_k|^2\}$,

$$\begin{aligned}\mathbb{E}\{|\boldsymbol{a}_k|^2\} &= \mathbb{E}^2\{\boldsymbol{a}_k\} + \mathbb{V}\{\boldsymbol{a}_k\} \\ &= \left(\sum_{m=1}^{M}\sqrt{\eta_{m,k}}\gamma_{m,k}\right)^2 + \sum_{m=1}^{M}\eta_{m,k}\beta_{m,k}\gamma_{m,k}\end{aligned} \tag{28}$$

Therefore, the optimization problem can be expressed as

$$\min_{\{\eta_{m,k}\}} \max_{\{k=1,\cdots,K\}} \frac{\mathbb{V}\{\tilde{\boldsymbol{a}}_k\}}{\mathbb{E}\{|\boldsymbol{a}_k|^2\}} \tag{29a}$$

$$\text{s.t.} \quad \eta_{m,k} \geq 0 \tag{29b}$$

$$\sum_{k=1}^{K}\eta_{m,k}\gamma_{m,k} \leq 1 \tag{29c}$$

$$\sigma^2_{x_k,y_k}(\boldsymbol{p}_{tx,k}) \leq \Gamma_{max} \tag{29d}$$

where Γ_{max} is the largest localization MSE the system can afford. The system does not allow the AP to use power from the other APs or the CPU, so that the the power control coefficient for the m-th AP to the k-th UE can not less than zero as shown in (29b). (29c) is the average power constraint for each AP that the m-th AP can not consume power exceed the power it has. (29d) is the requirement of radar localization error and the rational function of $\boldsymbol{p}_{tx,k}$ is quasiconvex not absolutely convex. Therefore, in order to compute the corresponding optimization problem by an appropriate search program, the constraint (29d) needs to be rewritten as [39]

$$\boldsymbol{Z}_{xy} = (\boldsymbol{r}_a + \boldsymbol{r}_b)^T - \Gamma_{max}(\boldsymbol{r}_a\boldsymbol{r}_b^T - \boldsymbol{r}_c\boldsymbol{r}_c^T)\boldsymbol{p}_{tx,k} \leq \boldsymbol{0} \tag{30}$$

To minimizing the maximum convex optimization objective, the min-max problem can be converted into a least value finding problem by introducing a value t that finding min t if $t \geq \frac{\mathbb{V}\{\tilde{\boldsymbol{a}}_k\}}{\mathbb{E}|\boldsymbol{a}_k|^2}$, the value t is the maximum value of the function (29a). Therefore, the problem (29) can be reformulated into an epigraph form:

$$\min_{\{\eta_{m,k},t\}} t \tag{31a}$$

$$\text{s.t.} \quad F_k(\eta_{m,k}) \leq tW_k(\eta_{m,k})Z_k(\eta_{m,k}) \tag{31b}$$

$$(29b), (29c), (30) \tag{31c}$$

where $F_k(\eta_{m,k}) = \sum_{m=1}^{M}\eta_{m,k}\beta_{m,k}\gamma_{m,k}$, $W_k(\eta_{m,k}) = 1 + \tau_{d,p}\rho_d\sum_{k'=1}^{K}\sum_{m=1}^{M}\eta_{m,k'}\beta_{m,k}\gamma_{m,k'}|\boldsymbol{\psi}_k^H\boldsymbol{\psi}_{k'}|^2$ and $Z_k(\eta_{m,k}) = \left(\sum_{m=1}^{M}\sqrt{\eta_{m,k}}\gamma_{m,k}\right)^2 + F_k(\eta_{m,k})$. Problem (31) is nonconvex since (30b) is neither convex nor concave with the respect to $\eta_{m,k}$, because of squaring a concave function $\sqrt{\eta_{m,k}}$ in term $Z_k(\eta_{m,k})$. Our idea is to reformulate problem (31) by approximating (31b) with successive convex approximation (SCA). Notice that since the min-max error objective can aslo be converted into a sum-error or weighted trade-offs problem within a linear transformation, these two could be tackled under the same framework.

A. Successive Convex Approximation (SCA) Method

The SCA is a linearization approach that replaces the non-convex term by its first-order Taylor expansion. Assume $\eta_{m,k}^{(n)}$ be the value of $\eta_{m,k}$ at the n-th iteration of the SCA algorithm, let $H_k(\eta_{m,k}) = tW_k(\eta_{m,k})Z_k(\eta_{m,k}) - F_k(\eta_{m,k})$, $z'_k(\eta_{m,k}) = \sum_{m=1}^{M}\sqrt{\eta_{m,k}}\gamma_{m,k}$ then the first-Taylor expansion of $H_k(\eta_{m,k})$ at point $\eta_{m,k}^{(n)}$ is

$$\begin{aligned}\tilde{H}_k(\eta_{m,k};\eta_{m,k}^{(n)}) &= H_k(\eta_{m,k}^{(n)}) + H_k^{(1)}(\eta_{m,k}^{(n)})(\eta_{m,k} - \eta_{m,k}^{(n)}) \\ &= \begin{cases} H_k(\eta_{m,k}^{(n)}) + \sum_{m,k'}[tZ_k\tau_{d,p}\rho_{d,p}\beta_{m,k'}\gamma_{m,k'}|\boldsymbol{\psi}_k^H\boldsymbol{\psi}_{k'}|^2 \\ \quad +tW_k(\frac{\gamma_{m,k}}{\sqrt{\eta_{m,k}}}z'_k + \beta_{m,k}\gamma_{m,k}) - \beta_{m,k}\gamma_{m,k}] \\ \quad *(\eta_{m,k} - \eta_{m,k}^{(n)}) & \text{if } k' = k, \\ H_k(\eta_{m,k}^{(n)}) + \sum_{m,k'}[tZ_k\tau_{d,p}\rho_{d,p}\beta_{m,k'}\gamma_{m,k'}|\boldsymbol{\psi}_k^H\boldsymbol{\psi}_{k'}|^2] \\ \quad *(\eta_{m,k} - \eta_{m,k}^{(n)}) & \text{otherwise} \end{cases}\end{aligned} \tag{32}$$

Proof. See Appendix C.

The constraint (30b) can be rewritten as

$$0 \leq \tilde{H}_k(\eta_{m,k};;\eta_{m,k}^{(n)}) \tag{33}$$

This leads to the optimization problem (33)

$$\min_{\{\eta_{m,k},t\}} t \tag{34a}$$

$$\text{s.t.} \quad (29b), (29c), (30), (33) \tag{34b}$$

If the value t is fixed, problem (34) is convex and can be efficiently solved by using interior point methods such as the bisection method [41]. The value t varies over an estimation error range $\{t_{min}, t_{max}\}$, which the range boundaries are computed based on the UL channel estimation. Within the interior point program such as the toolbox CVX [42][1], iterated steps, as shown in Algorithm 1, are developed by to find the optimal value t by adjusting the value of t_{min} and t_{max}. If the solving problem of (33) is convex feasibility, which means the predicted value t exists in the default range. Moreover, a true ratio check is used in the outer bisection iteration. By substituting the computed feasible values based on the local approximation into (31b), the variation of the value t will converge into a minimized value with the optimal power control coefficient $\eta_{m,k}$. According to (18), it is obviously that because of the pilot contamination, too much power of ISAC

[1]The first-order Taylor expansion of $Z_k(\eta_{m,k})$ which builds a new constraint $F_k(\eta_{m,k}) \leq tW_k(\eta_{m,k})\tilde{Z}_K^2(\eta_{m,k})$ gives a more global convex approximation because $f(x) = \sqrt{x}$ is an absolute concave function, whose first-order Taylor expansion is never smaller than the original function. However, CVX does not accept the "affine $\leq$ convex" constraint because of disciplined convex programming ruleset [42] even though it is mathematically true. Therefore, we raise the heuristic approximation based on $H_k(\eta_{m,k})$ in CVX.

Algorithm 1 SCA Bisection Algorithm for Solving (29)

Input: Given initial lower bound $t_{min} \leq t$ and upper bound $t_{max} \geq t$, set tolerance $\epsilon > 0$, initial power control coefficient $\eta_{m,k}^{(0)}$, maximum number of iteration I, i = 0
while $i \leq I$ **do**
  while $t_{max} - t_{min} \geq \epsilon$ **do**
    Set $t = (t_{max} + t_{min})/2$;
    Solve (34);
    if (34) is feasible for t $\forall k$ **then**
      Compute F_k^*, W_k^* and Z_k^* by $\eta_{m,k}^*$
      if (30b) is true for$t$ $\forall k$ **then**
        Set $t_{max} = t$, set $\eta_{m,k}^*$ as the solution to (34)
      else
        Set $t_{min} = t$
      end if
    else
      Set $t_{min} = t$
    end if
  end while
  Set $i = i + 1$, set $\eta_{m,k}^{(n)} = \eta_{m,k}^*$
end while
Output: $\eta_{m,k}^{(n)}$ and t

signal to one UE might affect the performance of other UEs as interference. Therefore, for the power constraints given in (29c), the system would not force each AP use all of its power to avoid the inter-signal interference. The algorithm is not only for power allocation but also optimization. However, when it comes to the full-power allocation strategy, the power control coefficient $\eta_{m,k}$ is fixed to $\sum_{k=1}^{K} \eta_{m.k}\gamma_{m,k} = 1$ in the DL transmission at the m-th AP.

Notice that when the optimization algorithm does not find a feasible solution to the ISAC system in DL transmission, no power control is performed. To avoid the no answer condition when there is no feasible solution, all the APs will transmit the DL training sequences with full power, without considering the requirements of radar localization.

B. Convergence Analysis

In this section, we analyze the convergence of the function of normalized channel estimation error, proving that by several times of iteration, the function converges to a certain value.

Define the convex set $\mathcal{C} = \{\eta_{m,k} \geq 0 : \sum_k \eta_{m,k}\gamma_{m,k} \leq 1, (\boldsymbol{r}_a + \boldsymbol{r}_b)^T - \Gamma_{max}(\boldsymbol{r}_a\boldsymbol{r}_b^T - \boldsymbol{r}_c\boldsymbol{r}_c^T)\boldsymbol{p}_{tx,k} \leq \boldsymbol{0}\}$. At the i-th iteration, we have the current iterate $\eta_{m,k}^{(i)} \in \mathcal{C}$ and the objective value $t^{(i)}$. Since $\left(\eta_{m,k}^{(i)}, t^{(i)}\right)$ is feasible in the convex inner-approximation, the $\min t$ solution is to obtain the best feasible next iterate that the problem can get while ensuring for all true $H_k \geq 0$, therefore the optimal $\left(\eta_{m,k}^{(i+1)}, t^{(i+1)}\right)$ satisfies

$$t^{(i+1)} = \min_{\substack{\eta_{m,k}\in\mathcal{C} \\ \tilde{H}_k(\eta_{m,k};\eta_{m,k}^{(n)})\geq 0}} t \leq t^{(i)} \tag{35}$$

which shows that sequence $\{t^{(1)}, t^{(2)}, \cdots, t^{(i)}\}$ is monotone non-increasing and bounded below by 0. Hence $t^{(i)} \to t^*$ exists finite as $i \to +\infty$.

Define $\varrho_{m,k}^{(i)}, \varsigma_k^{(i)}, \varpi_{p,q}^{(i)}$ and $\varepsilon_k^{(i)}$ are the Karush-Kuhn-Tucker (KKT) multipliers at the i-th iteration, the Lagragian of (31) can be expressed as

$$\begin{aligned}\mathcal{L}^{(i)}&(\eta_{m,k}^{(i)}, t^{(i)}; \varrho_{m,k}^{(i)}, \varsigma_k^{(i)}, \varpi_{p,q}^{(i)}, \varepsilon_k^{(i)}) \\ &= t^{(i)} + \sum_{m=1}^{M}\sum_{k=1}^{K} \varrho_{m,k}^{(i)}(-\eta_{m,k}^{(i)}) \\ &+ \sum_{m=1}^{M} \varsigma_m^{(i)}(\sum_{k=1}^{K} \eta_{m,k}\gamma_{m,k} - 1)^{(i)} \\ &+ \sum_{p=1}^{P}\sum_{q=1}^{q} \varpi_{p,q}^{(i)} Z_{xy}^{(i)} + \sum_{k=1}^{K} \varepsilon_k^{(i)}(-H_k(\eta_{m,k}^{(i)}))\end{aligned} \tag{36}$$

The full KKT system at the optimum $\left(\eta_{m,k}^{(i)}, t^{(i)}\right)$ of the convex SCA problem satisfies

$$\varrho_{m,k}^{(i)} \geq 0, \varsigma_k^{(i)} \geq 0, \varpi_{p,q}^{(i)} \geq 0, \varepsilon_k^{(i)} \geq 0 \tag{37a}$$

$$\varrho_{m,k}^{(i)}(\eta_{m,k}^{(i)}) = 0 \tag{37b}$$

$$\varsigma_m^{(i)}(\sum_{k=1}^{K} \eta_{m,k}\gamma_{m,k} - 1)^{(i)} = 0 \tag{37c}$$

$$\varpi_{p,q}^{(i)} Z_{xy}^{(i)} = 0 \tag{37d}$$

$$\varepsilon_k^{(i)}(\tilde{H}_k(\eta_{m,k}^{(i)})) = 0 \tag{37e}$$

$$\frac{\partial \mathcal{L}^{(i)}}{\partial \eta_{m,k}^{(i)}} = 0 \tag{37f}$$

$$\frac{\partial \mathcal{L}^{(i)}}{\partial t^{(i)}} = 0 \tag{37g}$$

Since the parameters and the multipliers are all in a bounded closed set, we assume that there exists $\eta_{m,k}^{(i)}, t^{(i)}, \varrho_{m,k}^{(i)}, \varsigma_k^{(i)}, \varpi_{p,q}^{(i)}, \varepsilon_k^{(i)} \to \bar{\eta}_{m,k}, \bar{t}, \bar{\varrho}_{m,k}, \bar{\varsigma}_k, \bar{\varpi}_{p,q}, \bar{\varepsilon}_k$ when $i \to +\infty$. For $\eta_{m,k}^{(i)} \to \bar{\eta}_{m,k}$, we have $H_k(\eta_{m,k}^{(i+1)}) \geq \tilde{H}_k(\eta_{m,k}^{(i+1)}; \eta_{m,k}^{(i)}) \geq 0$, therefore $H_k(\bar{\eta}_{m,k}) \geq 0$.

Because the other constraints can be rewritten into a linear continuous function, all the constraints can be passed to the limit to ensure the primal feasibility.

As the multipliers are all non-negative and convergent, $\bar{\varrho}_{m,k}, \bar{\varsigma}_k, \bar{\varpi}_{p,q}, \bar{\varepsilon}_k$ are non-negative as well. When $i \to +\infty$, we have $\varepsilon_k^{(i)}(\tilde{H}_k(\eta_{m,k}^{(i)})) \to \bar{\varepsilon}_k(H_k(\bar{\eta}_{m,k}))$. As a result, the complementary slackness $\varepsilon_k^{(i)}(\tilde{H}_k(\eta_{m,k}^{(i+1)}; \eta_{m,k}^{(i)})) = 0$ passes to $\bar{\varepsilon}_k H_k(\bar{\eta}_{m,k})) = 0$. The terms of the other multipliers follow the same pass.

For $\frac{\partial \mathcal{L}^{(i)}}{\partial \eta_{m,k}^{(i)}} = 0$ and $\frac{\partial \mathcal{L}^{(i)}}{\partial t^{(i)}} = 0$, notice that $\tilde{H}_k(\eta_{m,k}^{(i)}; \eta_{m,k}^{(i)}) = H_k(\eta_{m,k}^{(i)})$ and $\nabla\tilde{H}_k(\eta_{m,k}^{(i)}; \eta_{m,k}^{(i)}) = \nabla H_k(\eta_{m,k}^{(i)})$. Therefore, as $i \to +\infty$, we obtain $\frac{\partial \bar{\mathcal{L}}}{\partial \bar{\eta}_{m,k}} = 0$ and $\frac{\partial \bar{\mathcal{L}}}{\partial \bar{t}} = 0$.

It can be observed that these are the KKT conditions of the original problem at the certain solution point. In conclusion, any point $(\bar{\eta}_{m,k}, \bar{t})$ of the relaxed SCA function is a KKT solution of the original non-convex problem.

C. Power Map of Algorithm 1

The SCA-based scheme starts from the full-power scheme where the initial power allocation is based on the water-filling algorithm. With the proposed algorithm progressing,

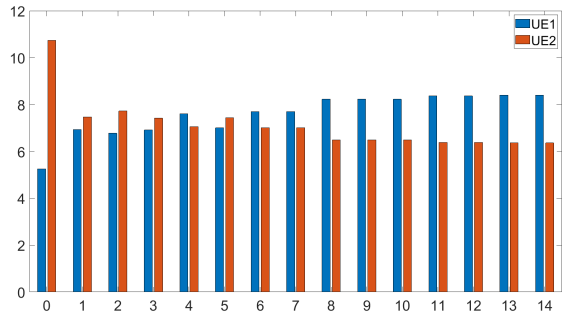

Fig. 2: Power map for two UEs on mirror positions, the CSI of one UE is half of the other.

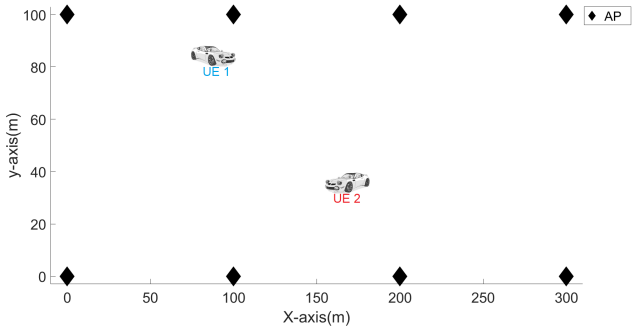

Fig. 3: Simulation scenario for ISAC performance.

the power allocation tends to steer toward weaker System-UE link until the system achieves the minimum maximum channel estimation error. The power map of two UEs are displayed in Fig.2. The UEs are set on mirror positions where both of them can be well served by all APs, within the CSI parameters of one UE is set half of the other.

IV. Simulation Evaluation

A. Parameters and Setup

In this section, the performances of the proposed strategy for channel estimation error and collaborative localization are evaluated. The impact of the channel estimation reliability on the DL data rate with MRT precoder is also demonstrated in this Section. When MRT is adopted, the signal-to-interference-plus-noise-ratio (SINR) and the data transmission rate are given by given by [43],

$$\mathrm{SINR}_k = \frac{e_k^2 \kappa P_{d,k}}{P_{d,k} + 1} \tag{38}$$

$$\mathrm{R}_k = B \log_2(1 + \mathrm{SINR}_k) \tag{39}$$

where $e_k^2 = \frac{\mathbf{E}\{|\boldsymbol{a}_k|^2\} - \mathbf{E}\{|\tilde{\boldsymbol{a}}_k|^2\}}{\mathbf{E}\{|\boldsymbol{a}_k|^2\}} = 1 - t$ indicates the reliability of the estimate, t represents the computed normalized channel estimation error which is the solution of the objective function (31a), and $P_{d,k}$ is the normalized power of downlink data payload. We assume that $P_{d,k}$ in each strategies and schemes keeps the same. The performances are also compared to the existing strategies. The influence of the pilot contamination in spare and denser networks are studied. We set a scenario for UEs, which are randomly deployed in a certain region, serving by APs for the performance analysis and comparison. The results are based on the different optimized power allocation schemes, focusing on the impact of ratio of DL/UL pilots and the total pilot length over the whole signal frames.

The scenario is a 300x100-square meter (m^2) dual-carriageway road on 2-D plane. The two served vehicles, UE1 and UE2 are separately deployed in different position in the area. The positions of each UE are randomly generated for 1000 times, which the average values are computed as the results for channel estimation performance, radar localization performance and power consumption. Eight APs are placed at both side of the road with equal deployment distance between each other, as shown in Fig.3.

The system bandwidth is 20 MHz, and carrier frequency is 2.4 GHz. 20 symbols are used as pilot training for either DL or UL. For the study on the impact of DL/UL ratio, the simulation begins when DL/UL ratio is 2:8, and then raises the length of the DL pilot sequence until 8:2 ratio. For the impact of pilot to the whole sequence length ratio, the simulation begins when the proportion on the pilot length to the entire frame length is 10%, and ends when the proportion is 50%. The DL/UL ratio of length is set to 5:5. When the number of pilot symbols is not integer, the number will be rounded up to the adjacent integer.

We assume that all the training sequences are generated with good orthogonality. The power of training symbols used in UL and DL are the same, which are 200 mW/symbol. Since the transmit power for both DL and UL depend on the length of the pilots, raising or reducing the length of DL and UL sequences affects the power constraints in DL and UL. Noise variance for UEs and radar receivers are assumed the same, which are -164 dBm/Hz.

The RCS model from transmitter AP to other receiver APs for radar sensing is set equal, that is, $|\mathbf{h}_{m_k}|^2$=0.85 for all $m \in \mathcal{M}$ and $k \in \mathcal{K}$. The localization error requirement is 1 m^2.

The three-slope model [44] is used for modeling the path loss and generate the large-scale fading coefficient $\beta_{m,k}$. Because of the random generation of channel values, the CSI of UEs at the certain position is generated for 500 times, the average values of the channel estimation error and localization error at the same position are chosen for representative analysis.

B. Simulation Results for DL/UL Ratio

Simulations in this section are carried out to evaluate the performance of the proposed DL pilot based ISAC strategy in the cell-free vehicular network within different DL/UL pilot ratios. The performance of the proposed strategy is compared to an existing strategy, which additional sequences of sensing symbols are contained in DL data signals [19]. Furthermore, to evaluate the performance of the proposed power allocation scheme, its performance is compared with the performance of a full-power power allocation scheme. As described in Section III., the proposed scheme aims to achieve communication and radar requirements with optimized power allocation. The full-power scheme is that all APs transmit with full power, within

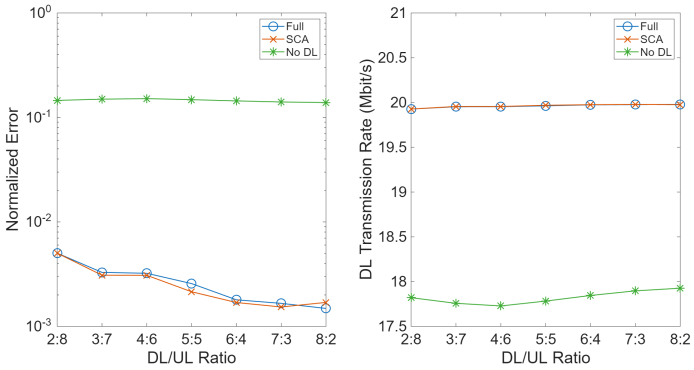

Fig. 4: (a) Variance of channel estimation error via DL/UL ratio. (b) DL data transmission via DL/UL ratio.

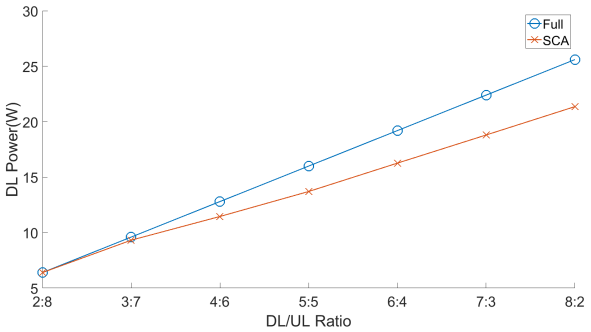

Fig. 6: DL power consumption via DL/UL ratio.

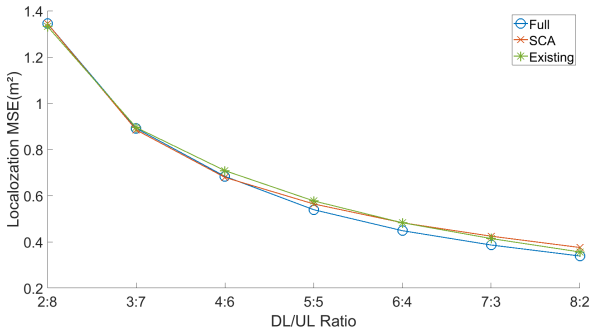

Fig. 5: Average localization error via DL/UL ratio.

radar and channel estimation sequences are allocated in equal power.

Fig.4 illustrates the communication performance between the proposed and existing cell-free ISAC system via the normalized variance of channel estimation error. The schemes of the two optimized and full-power allocation in DL pilot-based strategy are also studied.

As shown in Fig.4, "Full" represents the proposed ISAC strategy with the full-power allocation scheme. "SCA" indicates the proposed ISAC strategy with the SCA-based scheme at each AP, the number of UL and DL symbols are the same as the full-power. "No DL" stands for the conventional cell-free network that does not use DL training for channel estimation, within 20 UL pilot sequence length in order to compare the channel estimation performance under the same training length. All the simulations are carried out under the same condition.

By inserting the DL pilot sequences, the accuracy of channel estimation impoves approximately 1.5 orders of magnitude, as indicated by the below three lines in the figure. The substantial improvement comes from that the DL pilot-based strategy utilizing additional DL sequences for channel estimation. The transmission of these DL pilots takes into account the channel estimation errors arising from UL training phase, therefore leveraging the prior knowledge of CSI to further enhance the estimation accuracy. Consequently, even with an identical number of training sequences, the proposed strategy still significantly outperforms the existing conventional strategy.

It can be also observed that, after the ratio 6:4 point, the performance of the proposed system with the SCA-based scheme starts to get vibration, and at the ratio 8:2 point, the performance gets worse than the former 7:3 point and is surpassed by the full-power scheme. Although the DL pilot can offer significant improvement for the channel estimation, the CSI obtained during the UL training phase by UL pilots is also influential. UL training plays a key role in channel estimation. However, when a greater numbers of DL pilots are used for channel estimation, more resources are dedicated to the DL estimation, thereby enhancing the performance. Conversely, appointing further pilots to the DL diminishes the effectiveness of the UL channel estimation, ultimately leading to variability or even degradation in the overall system performance.

With regard to the performance of DL data transmission, Fig.4(b) illustrates that the proposed strategy improves around 10% of the DL data rate compared to the strategy without DL pilots. Although the normalized error with the proposed strategy decreases as the DL/UL ratio increases from 2:8 to 8:2, the improvement in DL data rate is relatively low. In contrast, despite only a slight reduction in normalized error for the traditional strategy, the DL data transmission exhibits a more obvious rise.

In Fig.5, with the best communication performance each system can achieve, the localization errors of proposed and existing strategies are shown, in order to evaluate the performance of the cell-free ISAC system in radar sensing. To compare the localization performance under the similar radar condition, the radar SNR is set the same for both ISAC strategies, i.e. $\text{SNR}_{\text{proposed}} = \text{SNR}_{\text{exi}}$. The results reflect the average cooperative localization error for the two UEs across random distributed positions. "Existing" refers to the ISAC strategy of the prior study which utilizes additional data sequences not the DL training sequences, under the same DL/UL ratio and radar SNR as the proposed strategy.

Although the system considers TDOA multiliteration estimator for user localization, our work focuses on the minimum mean square error the proposed system can achieve. Thus, the plotted MSE in the figures represents a lower bound. It is obviously that, when the DL/UL ratio is 2:8, none of the schemes satisfy the 1 m^2 localization error requirement, indicating that the resources allocated for the localization are insufficient. At the 4:6 ratio, the proposed strategy with full-power allocation starts to exhibit the best performance. At

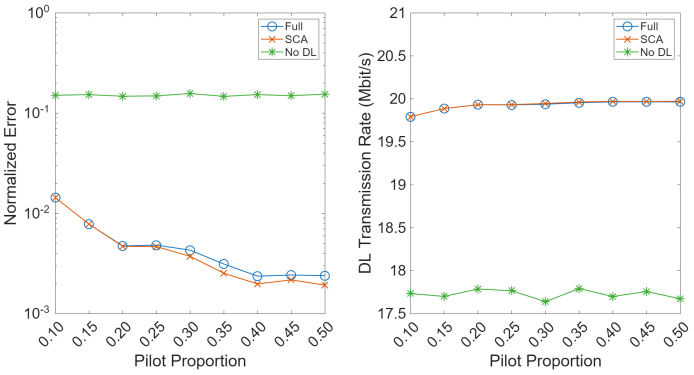

Fig. 7: (a) Variance of channel estimation error via pilot proportion. (b) DL data transmission via pilot proportion.

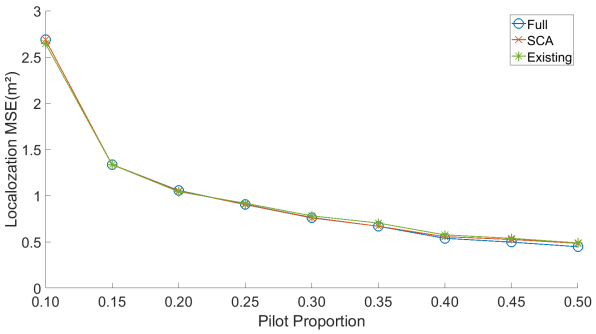

Fig. 8: Average localization error via pilot proportion.

the 6:4 ratio, the existing strategy begins to surpass the SCA-based scheme and achieves the second-best localization result among the four schemes. Although the existing work can achieve better work than the two optimized power allocation schemes in the proposed strategy under the certain conditions, it relies on the additional sequences used exclusively for radar sensing, which leads to a lower symbol efficiency compared to the proposed work. Regarding the proposed system in radar performance, it can be found that, the full-power scheme achieves the better results than the two optimized allocation schemes. This is because, without the interference caused by pilot reuse, more power allocated to radar function directly leads to higher SNR at the radar reiceiver side.

Fig.6 illustrates the power consumed by the proposed system during the DL training phase for both channel estimation and radar localization. Although the performance for the optimized power schemes cannot achieve better results than the full-power scheme on radar sensing localization at higher DL/UL ratios, the power required is less for the optimized schemes compared to full-power scheme. In particular, the SCA-based scheme reduces 17% of the power consumption at the ratio 8:2 point. In conclusion, when the DL sequences are with strong orthogonality and no pilot reuse occurs, the full-power allocation is preferable if the sensing is prioritized. Furthermore, we can also observe that the 6:4 point is a transition point at which the improvement brought by more DL pilots might no longer compensate for the performance degradation caused by the reduction of UL pilots.

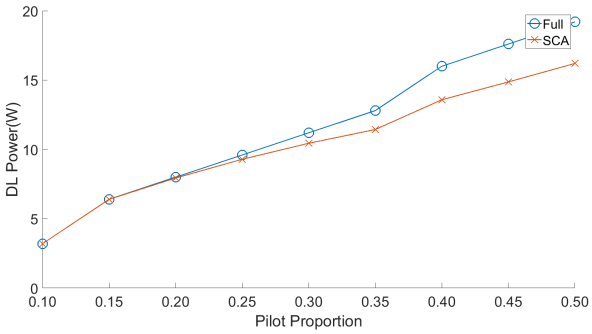

Fig. 9: Pilot power consumption via pilot proportion.

C. Simulation Results for Pilot Proportion

This section evaluates the performance for both communication and radar sensing of the proposed cell-free ISAC strategy under different pilot proportion on the pilot length to the entire frame length. The transmit power for both DL and UL maintain identical.

Fig.7(a) indicates that as the length of total pilot increases, which more symbols in DL phase are dedicated as pilots rather than data payloads, the performance of all power allocation schemes within the proposed strategy is improved until reaching the 0.4 proportion point. Beyond this point, the performance of SCA-based scheme is worsen and then improves again, while the performance for both full-power scheme is slightly getting worse. The results occur because at the point, the adverse influence from pilot contamination starts to counteract the benefits provided by the increased pilot symbols. Fig.7(b) shows that, under the proposed strategy, increasing the pilot proportion leads minimal impact on DL data transmission, while fluctuations in the traditional strategy reflect more prominently variability of the DL data transmission performance.

In Fig.8, it is evident that the cell-free ISAC system fails to meet the localization requirement until reaching the 0.25 proportion point, the solutions derived from the two optimized power allocation schemes are only local optimal. The performance of all schemes improves initially but the rate of improvement deminishes starting from the 0.40 proportion point.

Similarly as Fig.6, Fig.9 shows that the superior performance of the full-power allocation is accompanied by the cost of the highest power consumption. In contrast, calculating across all different pilot proportions, the SCA-based scheme consumes approximately 10% less power. In general, it can be observed that an easing point exists in the system regarding the pilot proportion. Upon reaching this point, allocating more additional symbols for ISAC functions yield a slight further improvement in the performance of either channel estimation or localization. Therefore, beyond the easing point, it becomes more practical to utilize the remaining frame resources for data transmission.

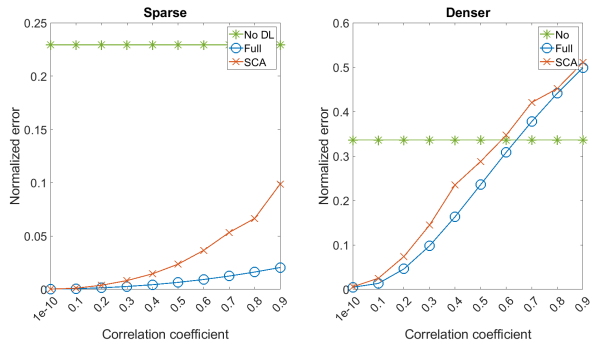

Fig. 10: (a) Sparse condition where two UEs are randomly distributed on the road. (b) Denser condition where six UEs are randomly distributed on the road.

D. Interference Analysis on pilot contamination

The previous simulation assumes that the ISAC sequences among UEs are within well orthogonal, however in practical environment, the DL-pilot contamination cannot be fully ignored. In this section, we study the influence of pilot contamination in sparse and dense UEs environment. The correlation coefficients among the DL-pilot sequences are set from the low contamination to high contamination.

As shown in Fig.10(a), when the pilot contamination gets worse, the performance of the SCA-based scheme degrades much compared to the full-power scheme. The performance of the proposed system still demonstrates better performance over the traditional cell-free ISAC system under both power allocation schemes. However, Fig.10(b) reveals that when the correlation coefficient reaches 0.6, the performance of the proposed system within the SCA-based scheme becomes inferior to that of the traditional system, and beyond this value, the proposed system performs worse than the traditional. It is also obviously that the number of UEs affects the severity of the pilot contamination, as a denser environment leads to a more pronounced performance degradation.

V. Conclusions

In this paper, we analyzed the performance for both communication and radar sensing within DL training phase in the cell-free ISAC networks. A power allocation scheme was proposed to minimize the maximum communication channel estimation while satisfying both the requirement of radar localization and per-AP power constraints. Furthermore, the impact of DL/UL pilot ratio and of pilot length over the whole signal frames to the performance of the proposed ISAC strategy were studied. The simulation results showed that by inserting additional pilot sequences for DL training, both channel estimation and radar localization accuracy were significantly improved compared to the existing studies with either optimized or full-power allocation scheme. The full-power allocation performed better than the optimized, however, more consumed power during DL training phase led to less power for the following data transmission phase when the total power of the system was constrained. Furthermore, there is a turning point of the system on channel estimation performance on the ratio between the DL length and the UL length that longer DL but the shorter UL pilot will lead to worse performance of channel estimation. An easing point was also given that neither channel estimation nor localization will be much improved even with more pilots. Additional, the impact on DL data transmission performance is minimal at low normalized error values, while the influence on DL data performance is more pronounced as the normalized error remains high.

VI. Appendix

A. Proof of (4)

To derive the linear MMSE estimator of the random variable $g_{m,k}$ based on the observed $\check{\mathbf{y}}_{u_{m,k}}$, we compute

$$\begin{aligned}\hat{g}_{m,k} &= \frac{\mathrm{Cov}\{g_{m,k},\check{\mathbf{y}}_{u_{m,k}}\}}{\mathbb{V}\{\check{\mathbf{y}}_{u_{m,k}}\}}(\check{\mathbf{y}}_{u_{m,k}}-\mathbb{E}\{\check{\mathbf{y}}_{u_{m,k}}\})+\mathbb{E}\{g_{m,k}\}\\ &=\frac{\mathbb{E}\left\{\check{\mathbf{y}}^*_{u_{m,k}}g_{m,k}\right\}-\mathbb{E}\left\{\check{\mathbf{y}}^*_{u_{m,k}}\right\}\mathbb{E}\left\{g_{m,k}\right\}}{\mathbb{E}\left\{|\check{\mathbf{y}}^*_{u_{m,k}}|^2\right\}-\left(\mathbb{E}\left\{\check{\mathbf{y}}^*_{u_{m,k}}\right\}\right)^2}(\check{\mathbf{y}}_{u_{m,k}}-\mathbb{E}\{\check{\mathbf{y}}_{u_{m,k}}\})\\ &+\mathbb{E}\{g_{m,k}\}\\ &=\frac{\mathbb{E}\left\{\check{\mathbf{y}}^*_{u_{m,k}}g_{m,k}\right\}}{\mathbb{E}\left\{|\check{\mathbf{y}}_{u_{m,k}}|^2\right\}}\check{\mathbf{y}}_{u_{m,k}}\\ &=\frac{\mathbb{E}\left\{A\sqrt{\beta_{m,k}}h_{m,k}+B\sqrt{\beta_{m,k}}h_{m,k}+C\sqrt{\beta_{m,k}}h_{m,k}\right\}}{\mathbb{E}\left\{A^2+B^2+C^2+2AB+2AC+2BC\right\}}\check{\mathbf{y}}_{u_{m,k}}\end{aligned} \tag{40}$$

where $A=\sqrt{\tau_{u,p}\rho_{u,p}}\sqrt{\beta_{m,k}}h_{m,k}$, $B=\sqrt{\tau_{u,p}\rho_{u,p}}\sum_{k'\neq k}^{K}\sqrt{\beta_{m,k'}}h_{m,k'}\boldsymbol{\phi}_k^H$, $C=\boldsymbol{\phi}_k^H\boldsymbol{w}_{u_m}$. Note that random variables $h_{m,k}$ and w_{u_k} are independent, and are $\sim\mathcal{CN}(0,1)$.

$$\mathbb{E}\left\{|h_{m,k}|^2\right\}=\mathbb{V}\left\{h_{m,k}\right\}+|\mathbb{E}\left\{h_{m,k}\right\}|^2=1 \tag{41}$$

$$\mathbb{E}\left\{|w_{u_k}|^2\right\}=\mathbb{V}\left\{w_{u_k}\right\}+|\mathbb{E}\left\{w_{u_k}\right\}|^2=1 \tag{42}$$

Finally, substituting (34) and (35) into (33), we obtain the MMSE estimation of the estimated UL CSI as in (4).

B. Proof of (6)

The estimated channel gain $\hat{g}_{m,k}$ and the error $\tilde{g}_{m,k}$ are uncorrelated and statistically independent, both of them are Gaussian distributed and have zero-mean. Thus, we compute

$$\begin{aligned}\mathbb{V}\{g_{m,k}\}&=\mathbb{V}\{\tilde{g}_{m,k}+\hat{g}_{m,k}\}\\ &=\mathrm{Cov}((\tilde{g}_{m,k}+\hat{g}_{m,k}),(\tilde{g}_{m,k}+\hat{g}_{m,k}))\\ &=\mathrm{Cov}(\tilde{g}_{m,k},(\tilde{g}_{m,k}+\hat{g}_{m,k}))+\\ &\quad\mathrm{Cov}(\hat{g}_{m,k},(\tilde{g}_{m,k}+\hat{g}_{m,k}))\\ &=\mathrm{Cov}(\tilde{g}_{m,k},\tilde{g}_{m,k})+\mathrm{Cov}(\hat{g}_{m,k},\hat{g}_{m,k})+\\ &\quad 2\mathrm{Cov}(\tilde{g}_{m,k},\hat{g}_{m,k})\\ &=\mathbb{V}\{\tilde{g}_{m,k}\}+\mathbb{V}\{\hat{g}_{m,k}\}\end{aligned} \tag{43}$$

Then

$$\begin{aligned}\mathbb{V}\{\tilde{g}_{m,k}\}&=\mathbb{V}\{g_{m,k}\}-\mathbb{V}\{\hat{g}_{m,k}\}\\ &=\mathbb{E}\{(g_{m,k}-\mathbb{E}\{g_{m,k}\})^2\}-\mathbb{E}\{(\hat{g}_{m,k}-\mathbb{E}\{\hat{g}_{m,k}\})^2\}\\ &=\mathbb{E}\{(\sqrt{\beta_{m,k}}h_{m,k})^2\}-\mathbb{E}\{(\hat{g}_{m,k})^2\}\end{aligned} \tag{44}$$

By substituting (5) and (34) into (37), we have the variance of the estimated channel error as in (6).

C. Proof of (32)

To apply the first-order Taylor expansion on $H_k(\eta_{m,k})$, we need to compute its gradient. With the product rule, the gradient of $H_k(\eta_{m,k})$ can be expressed as

$$\begin{aligned}\frac{\partial H_k}{\partial \eta_{m,k'}} &= t\frac{\partial (W_k Z_k)}{\partial \eta_{m,k'}} - \frac{\partial F_k}{\partial \eta_{m,k'}} \\ &= t\left[\frac{\partial W_k}{\partial \eta_{m,k'}} Z_k + \frac{\partial Z_k}{\partial \eta_{m,k'}} W_k\right] - \frac{\partial F_k}{\partial \eta_{m,k'}}\end{aligned} \tag{45}$$

When $k' \neq k$, the term F_k and $z_k'(\eta_{m,k})$ in Z_k do not depend on $\eta_{m,k'}$, therefore

$$\frac{\partial F_k}{\partial \eta_{m,k'}} = \begin{cases} \beta_{m,k}\gamma_{m,k} & \text{if } k' = k, \\ 0 & \text{otherwise} \end{cases} \tag{46}$$

$$\frac{\partial Z_k}{\partial \eta_{m,k'}} = \begin{cases} \frac{\gamma_{m,k}}{\sqrt{\eta_{m,k}}} z_k' + \beta_{m,k}\gamma_{m,k} & \text{if } k' = k, \\ 0 & \text{otherwise} \end{cases} \tag{47}$$

And always

$$\frac{\partial W_k}{\eta_{m,k'}} = \tau_{d,p}\rho_{d,p}\beta_{m,k'}\gamma_{m,k'}|\boldsymbol{\psi}_k^H \boldsymbol{\psi}_{k'}|^2 \tag{48}$$

As a result, by substituting (52), (53) and (54) into (51), when $k' = k$, we can derive the final gradient as

$$\begin{aligned}\frac{\partial H_k}{\partial \eta_{m,k'}} &= t[Z_k \tau_{d,p}\rho_{d,p}\beta_{m,k'}\gamma_{m,k'}|\boldsymbol{\psi}_k^H \boldsymbol{\psi}_{k'}|^2 \\ &\quad + W_k(\frac{\gamma_{m,k}}{\sqrt{\eta_{m,k}}} z_k' + \beta_{m,k}\gamma_{m,k})] - \beta_{m,k}\gamma_{m,k}\end{aligned} \tag{49}$$

REFERENCES

[1] M. H. Miraz, M. Ali, P. S. Excell, and R. Picking, "A review on internet of things (IoT), internet of everything (IoE) and internet of nano things (IoNT)," in *2015 Internet Technologies and Applications (ITA)*, 2015, pp. 219–224.

[2] W. Saad, M. Bennis, and M. Chen, "A vision of 6G wireless systems: Applications, trends, technologies, and open research problems," *IEEE Network*, vol. 34, no. 3, pp. 134–142, 2020.

[3] W. Yuan, Z. Wei, S. Li, J. Yuan, and D. W. K. Ng, "Integrated sensing and communication-assisted orthogonal time frequency space transmission for vehicular networks," *IEEE Journal of Selected Topics in Signal Processing*, vol. 15, no. 6, pp. 1515–1528, 2021.

[4] Z. Huang, K. Wang, A. Liu, Y. Cai, R. Du, and T. X. Han, "Joint pilot optimization, target detection and channel estimation for integrated sensing and communication systems," *IEEE Transactions on Wireless Communications*, vol. 21, no. 12, pp. 10 351–10 365, 2022.

[5] M. Temiz, N. J. Peters, C. Horne, M. A. Ritchie, and C. Masouros, "Radar-centric isac through index modulation: Over-the-air experimentation and trade-offs," in *2023 IEEE Radar Conference (RadarConf23)*, 2023, pp. 1–6.

[6] Z. Lyu, L. Zhang, H. Zhang, Z. Yang, H. Yang, N. Li, L. Li, V. Bobrovs, O. Ozolins, X. Pang, and X. Yu, "Radar-centric photonic terahertz integrated sensing and communication system based on lfm-psk waveform," *IEEE Transactions on Microwave Theory and Techniques*, vol. 71, no. 11, pp. 5019–5027, 2023.

[7] K. Gu, Y. Wang, and Y. Shen, "Cooperative detection by multi-agent networks in the presence of position uncertainty," *IEEE Transactions on Signal Processing*, vol. 68, pp. 5411–5426, 2020.

[8] H. L. Van Trees, *Detection, estimation, and modulation theory, part I: detection, estimation, and linear modulation theory*. John Wiley & Sons, 2004.

[9] O. Kanhere, S. Goyal, M. Beluri, and T. S. Rappaport, "Target localization using bistatic and multistatic radar with 5G NR waveform," in *2021 IEEE 93rd Vehicular Technology Conference (VTC2021-Spring)*, 2021, pp. 1–7.

[10] S. R. Doughty, *Development and performance evaluation of a multistatic radar system*. University of London, University College London (United Kingdom), 2008.

[11] H. Q. Ngo, A. Ashikhmin, H. Yang, E. G. Larsson, and T. L. Marzetta, "Cell-free massive MIMO: Uniformly great service for everyone," in *2015 IEEE 16th International Workshop on Signal Processing Advances in Wireless Communications (SPAWC)*, 2015, pp. 201–205.

[12] ——, "Cell-free massive MIMO versus small cells," *IEEE Transactions on Wireless Communications*, vol. 16, no. 3, pp. 1834–1850, 2017.

[13] H. A. Ammar, R. Adve, S. Shahbazpanahi, G. Boudreau, and K. V. Srinivas, "User-centric cell-free massive MIMO networks: A survey of opportunities, challenges and solutions," *IEEE Communications Surveys Tutorials*, vol. 24, no. 1, pp. 611–652, 2022.

[14] J. A. Zhang, K. Wu, X. Huang, Y. J. Guo, D. Zhang, and R. W. Heath, "Integration of radar sensing into communications with asynchronous transceivers," *IEEE Communications Magazine*, vol. 60, no. 11, pp. 106–112, 2022.

[15] Y.-C. Wu, Q. Chaudhari, and E. Serpedin, "Clock synchronization of wireless sensor networks," *IEEE Signal Processing Magazine*, vol. 28, no. 1, pp. 124–138, 2011.

[16] R. Rogalin, O. Y. Bursalioglu, H. Papadopoulos, G. Caire, A. F. Molisch, A. Michaloliakos, V. Balan, and K. Psounis, "Scalable synchronization and reciprocity calibration for distributed multiuser MIMO," *IEEE Transactions on Wireless Communications*, vol. 13, no. 4, pp. 1815–1831, 2014.

[17] V. S. Chernyak, *Fundamentals of multisite radar systems: multistatic radars and multistatic radar systems*. Routledge, 2018.

[18] U. Demirhan and A. Alkhateeb, "Cell-free ISAC MIMO systems: Joint sensing and communication beamforming," *IEEE Transactions on Communications*, pp. 1–1, 2024.

[19] Z. Behdad, T. Demir, K. W. Sung, E. Björnson, and C. Cavdar, "Multistatic target detection and power allocation for integrated sensing and communication in cell-free massive MIMO," *IEEE Transactions on Wireless Communications*, vol. 23, no. 9, pp. 11 580–11 596, 2024.

[20] E. Björnson, E. G. Larsson, and M. Debbah, "Massive MIMO for maximal spectral efficiency: How many users and pilots should be allocated?" *IEEE Transactions on Wireless Communications*, vol. 15, no. 2, pp. 1293–1308, 2016.

[21] H. Q. Ngo and E. G. Larsson, "No downlink pilots are needed in tdd massive MIMO," *IEEE Transactions on Wireless Communications*, vol. 16, no. 5, pp. 2921–2935, 2017.

[22] Z. Chen and E. Björnson, "Channel hardening and favorable propagation in cell-free massive MIMO with stochastic geometry," *IEEE Transactions on Communications*, vol. 66, no. 11, pp. 5205–5219, 2018.

[23] J. Zhang, S. Chen, Y. Lin, J. Zheng, B. Ai, and L. Hanzo, "Cell-free massive MIMO: A new next-generation paradigm," *IEEE Access*, vol. 7, pp. 99 878–99 888, 2019.

[24] G. Interdonato, H. Q. Ngo, P. Frenger, and E. G. Larsson, "Downlink training in cell-free massive MIMO: A blessing in disguise," *IEEE Transactions on Wireless Communications*, vol. 18, no. 11, pp. 5153–5169, 2019.

[25] A. Sakhnini, M. Guenach, A. Bourdoux, H. Sahli, and S. Pollin, "A target detection analysis in cell-free massive MIMO joint communication and radar systems," in *ICC 2022 - IEEE International Conference on Communications*, 2022, pp. 2567–2572.

[26] M. E. Knox, "Single antenna full duplex communications using a common carrier," in *WAMICON 2012 IEEE Wireless Microwave Technology Conference*, 2012, pp. 1–6.

[27] H. Nawaz and I. Tekin, "Double-differential-fed, dual-polarized patch antenna with 90 dB interport RF isolation for a 2.4 GHz in-band full-duplex transceiver," *IEEE Antennas and Wireless Propagation Letters*, vol. 17, no. 2, pp. 287–290, 2018.

[28] W. Zhou, R. Zhang, G. Chen, and W. Wu, "Integrated sensing and communication waveform design: A survey," *IEEE Open Journal of the Communications Society*, vol. 3, pp. 1930–1949, 2022.

[29] Y. Huang, S. Hu, S. Ma, Z. Liu, and M. Xiao, "Designing low-PAPR waveform for OFDM-based RadCom systems," *IEEE Transactions on Wireless Communications*, vol. 21, no. 9, pp. 6979–6993, 2022.

[30] S. M. Kay, "Fundamentals of statistical signal processing: Estimation theory," 1993.

[31] M. A. Richards, J. Scheer, W. A. Holm, and W. L. Melvin, "Principles of modern radar," 2010.

[32] H. Chen, H. Sarieddeen, T. Ballal, H. Wymeersch, M.-S. Alouini, and T. Y. Al-Naffouri, "A tutorial on terahertz-band localization for 6G communication systems," *IEEE Communications Surveys Tutorials*, vol. 24, no. 3, pp. 1780–1815, 2022.
[33] Y. Chan and K. Ho, "A simple and efficient estimator for hyperbolic location," *IEEE Transactions on Signal Processing*, vol. 42, no. 8, pp. 1905–1915, 1994.
[34] Y. Sun, K. C. Ho, and Q. Wan, "Solution and analysis of TDOA localization of a near or distant source in closed form," *IEEE Transactions on Signal Processing*, vol. 67, no. 2, pp. 320–335, 2019.
[35] G. Shen, R. Zetik, and R. S. Thoma, "Performance comparison of TOA and TDOA based location estimation algorithms in LOS environment," in *2008 5th Workshop on Positioning, Navigation and Communication*, 2008, pp. 71–78.
[36] B. Hao, Y. Zhao, Z. Li, and P. Wan, "A sensor selection method for TDOA and AOA localization in the presence of sensor errors," in *2017 IEEE/CIC International Conference on Communications in China (ICCC)*, 2017, pp. 1–6.
[37] Y. C. Eldar *et al.*, "Rethinking biased estimation: Improving maximum likelihood and the Cramér–Rao bound," *Foundations and Trends® in Signal Processing*, vol. 1, no. 4, pp. 305–449, 2008.
[38] E. S. Crafts, X. Zhang, and B. Zhao, "Bayesian Cramér-Rao bound estimation with score-based models," *IEEE Transactions on Information Theory*, pp. 1–1, 2024.
[39] H. Godrich, A. P. Petropulu, and H. V. Poor, "Power allocation strategies for target localization in distributed multiple-radar architectures," *IEEE Transactions on Signal Processing*, vol. 59, no. 7, pp. 3226–3240, 2011.
[40] A. Ahmed and Y. D. Zhang, "Optimized resource allocation for distributed joint radar-communication system," *IEEE Transactions on Vehicular Technology*, vol. 73, no. 3, pp. 3872–3885, 2024.
[41] S. Boyd and L. Vandenberghe, *Convex optimization*. Cambridge university press, 2004.
[42] M. Grant and S. Boyd, "CVX: Matlab software for disciplined convex programming, version 2.1," https://cvxr.com/cvx, Mar. 2014.
[43] F. Rusek, D. Persson, B. K. Lau, E. G. Larsson, T. L. Marzetta, O. Edfors, and F. Tufvesson, "Scaling up MIMO: Opportunities and challenges with very large arrays," *IEEE Signal Processing Magazine*, vol. 30, no. 1, pp. 40–60, 2013.
[44] A. Tang, J. Sun, and K. Gong, "Mobile propagation loss with a low base station antenna for NLOS street microcells in urban area," in *IEEE VTS 53rd Vehicular Technology Conference, Spring 2001. Proceedings (Cat. No.01CH37202)*, vol. 1, 2001, pp. 333–336 vol.1.